ACS Photonics

Article

Cite This: ACS Photonics 2018, 5, 3198−3204

Revisitation of Extraordinary Young's Interference: from Catenary Optical Fields to Spin−Orbit Interaction in Metasurfaces

Mingbo Pu, Yinghui Guo, Xiong Li, Xiaoliang Ma, and Xiangang Luo*

State Key Laboratory of Optical Technologies on Nano-Fabrication and Micro-Engineering, Institute of Optics and Electronics, Chinese Academy of Sciences, Chengdu 610209, China

University of Chinese Academy of Sciences, Beijing 100049, China

ABSTRACT: Extraordinary Young's interference is an anomalous phenomenon observed at metallic surface in 2004. The shrinkage of slit size into deep subwavelength scale introduces many novel effects that cannot be described by classic interference theory. In this paper, the Young's interference excited by subwavelength slits is investigated via rigorous Maxwell's equations. We reveal a universal spin−orbit interaction mechanism associated with the catenary optical fields in 2D isotropic metal-dielectric structures for the generation of optical vortex array and spin Hall effect. Based on the interference of vectorial vortex arrays with opposite topological charges, a simple yet powerful method for the fabrication of space-variant metasurfaces is proposed for the first time, which breaks the fundamental limit of traditional interference lithography. These results may provide numerous new perspectives on both the design of catenary metasurfaces and optical spin-controlled devices.

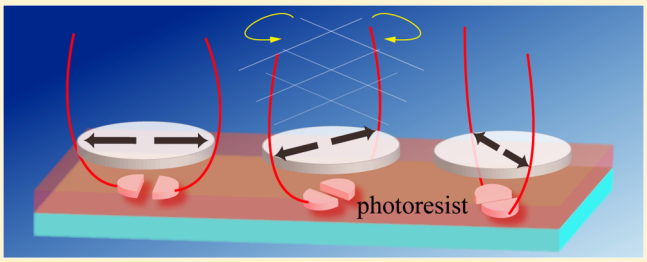

KEYWORDS: *interference, metasurface, catenary optics, spin−orbit interaction, nanolithography*

As one of the most beautiful experiments in physics,[1] Young's double slits interference provides a general platform for the investigation of light, sound, and matter waves. Actually, interference serves as the basis of other fundamental wave phenomena including refraction, reflection and diffraction.[2] However, classic interference relies on the propagative accumulation of phase delay via $\Delta\Phi = 2\pi l/\lambda$, where l is the propagation length and λ is the wavelength. When λ is very large compared to l, no obvious interference can be observed. As a result, the interference period of counter-propagating light is limited to $\lambda/2$. As Ernst Abbe pointed out in 1873, the highest spatial resolution of optical microscopy is just $\lambda/2$, which sets a fundamental barrier known as diffraction limit.[3,4] On the other hand, a minimal thickness of $\lambda/4$ is required for interferential reduction of Fresnel reflection, which constrained the compactness of devices especially for long wavelengths.[5] In addition, although multiphoton absorption could reduce the interference patterns by N-times,[6] the lack of practical N-photon absorbing resist restricts their engineering applications.[7,8]

Subwavelength Young's interference of classic light in metallic structures was discovered in 2004.[9,10] During the investigation of interference of light emerged from nanoslits on silver films, it was experimentally observed that the interference period shrunk from the normal $\lambda/2$ to smaller than $\lambda/4$. This unexpected interference phenomenon, known as extraordinary Young's interference (EYI),[8] was astonishing since neither entangled light nor high index materials were used. Theoretical analysis shows that the shrinkage of interference pattern is associated with the collective excitation of free electrons on the metallic surface, that is, the surface plasmon polaritons (SPPs). The dispersion relation of SPPs indicates that the thinner the metallic film, the shorter the effective wavelength can be obtained.[10] Based on this property, it was predicted and later demonstrated that interference period smaller than $\lambda/8$ is possible.[10,11]

In classic Young's experiment, the transmission efficiency of light is often thought to be proportional to the occupied area of the slits. However, at the subwavelength scale, the transmission through nanoslits is related to the distance between adjacent slits owing to the interference of SPPs propagating on the surface. Schouten et al. experimentally investigated the periodic fluctuation of transmission with respect to the slits distance,[12] demonstrating that a full-vectorial analysis of the subwavelength Young's interference is required. Subsequently, inspired by the thickness-dependent plasmonic coupling on metallic thin films,[10] the width of nanoslits was varied to result a horizontal shift of the interference patterns, which provides an efficient mean to modulate the phase of electromagnetic oscillation in both free space and at the metallic surfaces.[13−15] Zia et al., also performed a double-slit experiment with SPPs to reveal the strong analogy between SPPs propagating along the surface of metallic structures and light propagating in conventional dielectric components.[16] Based on these pioneering work,

Received: April 6, 2018
Published: June 20, 2018

DOI: 10.1021/acsphotonics.8b00437
ACS Photonics 2018, 5, 3198−3204

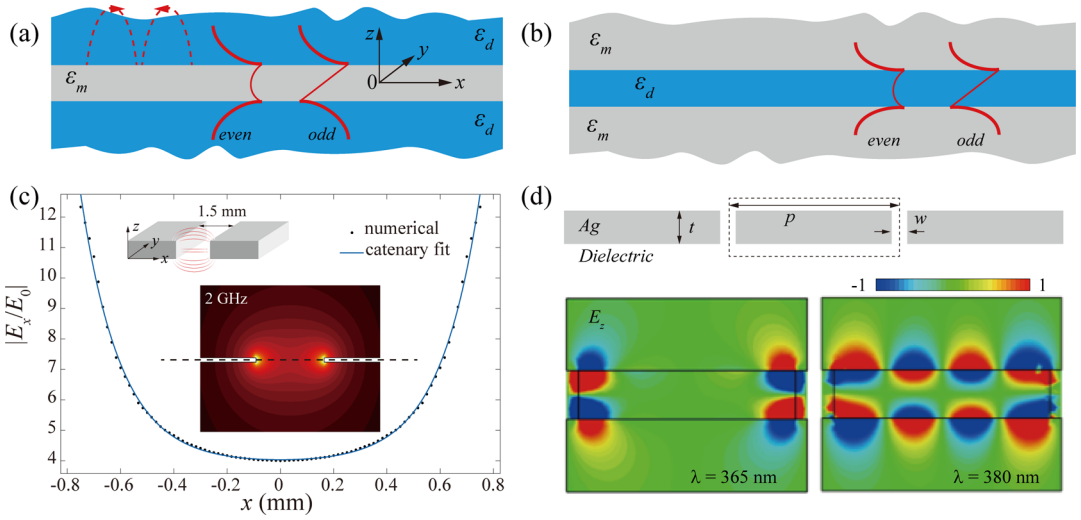

Figure 1. Catenary optical fields in subwavelength structures. (a, b) Coupled plasmonic modes in metal-dielectric stacks. The dashed lines show the electric force lines with a shape of "catenary of equal phase gradient". The solid curves show the amplitude of E_x for even and odd modes. For even mode, E_x follows a catenary function. For odd mode, H_y and E_z have a catenary shape. (c) Normalized E_x between two metallic sheets made of perfect electric conductor (numerical), as well as the curve fitted using hyperbolic cosine function (catenary fit). The fitted value for α is 6.639 mm^{-1}, which is about 158× the vacuum wavenumber at 2 GHz. (d) Top panel shows the basic configuration of Young's interference experiment, while the dashed rectangle indicates the simulation region. The bottom figure shows the instantaneous E_z at 365 and 380 nm. Here p, w, and t are set as 100, 10, and 20 nm. The refractive index of the dielectric is 1.7.

various functional devices, such as plasmonic lenses and waveguides, beam shapers, as well as orbital angular momentum generators, have been realized by various groups.[17−20]

Thus far, most results on the Young's interference were obtained with 1D slits. In this paper, we shall study the Young's interference with complex nanoslits, which certainly possesses more physical meanings. Based on the catenary optical fields proposed in the following, strong spin−orbit interaction and spin Hall effect are observed in the form of vertically polarized optical vortexes. By exploiting the interference of two opposite circularly polarized light (CPL), a simple approach for nanofabrication of inhomogeneous metasurface is presented for the first time, which breaks the limit of traditional interference lithography.[9,21,22]

RESULTS AND DISCUSSION

Theory of Catenary Optical Fields. In order to understand the EYI effect, the electromagnetic fields in metallic thin films and subwavelength slits therein must be considered from a fundamental level described by Maxwell's equations. For source-free and nonmagnetic system, the Maxwell wave equations can be written as[8]

$$\nabla^2\mathbf{E} + \nabla\left[\mathbf{E}\cdot\frac{\nabla\varepsilon}{\varepsilon}\right] + k_0^2\varepsilon\mu\mathbf{E} = 0,$$
$$\nabla^2\mathbf{H} + \frac{\nabla\varepsilon}{\varepsilon}\times(\nabla\times\mathbf{H}) + k_0^2\varepsilon\mu\mathbf{H} = 0 \quad (1)$$

where $\mathbf{E}$ and $\mathbf{H}$ are the electric and magnetic fields, ε and μ are the permittivity and permeability of constitutive materials, k_0 is the wavenumber in free space. The second terms in eq 1 are responsible for the polarization coupling induced by an abrupt change in the dielectric constant. For homogeneous constitutive materials ($\nabla\varepsilon = 0$) or 2D structures,[23] the polarization coupling terms are zero, thus, eq 1 reduces to ordinary Helmholtz equations. In general, complex electromagnetic problems can be either solved using eq 1 or through the combination of Helmholtz equations and boundary conditions.

The Helmholtz equations for multilayered system, such as that shown in Figure 1a,b, can be solved using separation of variables. Taking the transverse magnetic (TM) polarized SPPs as an example, the fields inside the core are a summation of two counter-propagating evanescent waves:

$$E_x \propto A\ \exp(i\beta x + \alpha z) + B\ \exp(i\beta x - \alpha z) \quad (2)$$

where β and $\alpha = ik_z$ are the propagation and attenuation constants related by $\beta^2 = \alpha^2 + \varepsilon k_0^2$, ε is the permittivity of core material, and A and B are coefficients. When the structures are symmetric, A and B should be equal in amplitude, but the sign may be different dependent on the symmetry of modes. For symmetric (even) mode, the instantaneous E_x has a catenary shape (hyperbolic cosine function), which is symmetric with respect to $z = 0$:

$$E_x \propto \exp(\alpha z) + \exp(-\alpha z) = 2\cosh(\alpha z) \quad (3)$$

while E_z and H_y follow an antisymmetric (odd) hyperbolic sine function. Obviously, the catenary optical field is an intrinsic mode resulting from the evanescent coupling, which must be considered in subwavelength metallic slits and films. From another viewpoint, this catenary-shaped field is coincident with the physics behind the mechanical catenary, because both of them could be interpreted using the minimal potential energy principle and the variational theorem.[24]

The catenary optical fields also exist in cases where the polarization coupling cannot be neglected, if proper boundary conditions are considered. For instance, the microwave fields in the gap between two thin metallic sheets can be written in a catenary shape. Figure 1c illustrates the schematic and calculated electric fields at 2 GHz (λ = 150 mm) for an infinite long slit with a width of 1.5 mm and thickness of 0.1 mm. At this low frequency, metal can be treated as perfect electric conductor and SPPs do not exist. The magnitude of the E_x along the center of the slit is given together with a curve

DOI: 10.1021/acsphotonics.8b00437
ACS Photonics 2018, 5, 3198−3204

fitted using the catenary function, and excellent agreement is found.

Another interesting effect of the catenary optical field in the microwave regime lies in the fact that the intensity is dependent on the slit width, similar to the SPPs in the visible region,[14] implying that there is a deep link between the optical and microwave phenomena.[25] In fact, they share a lot of common ground and belong to the same concept of metasurface wave (M-wave).[26] Since this is not the target of this paper, we would like to address it elsewhere.

Subwavelength Young's Interference. The catenary optical fields have strong influence on the double slits interference. As shown in Figure 1d, two 10 nm wide nanoslits are used to excite the EYI on a 20 nm thick silver film. Under x-polarized incidence, antisymmetric E_z is generated with a hyperbolic sine shaped amplitude profile. When the wavelength increases from λ = 365 to 380 nm, the interference period anomalously decreases from 100 nm to about 25 nm, which implies that one may increase the optical resolution without reducing the wavelength. This is coincident with the recent development of plasmonic nanolithographic systems.[27]

Besides the deep subwavelength interference period, the interference patterns could be controlled by introducing more complex metal-dielectric structures such as multilayers and meta-mirrors.[28,29] As shown in Figure 2a, an additional aluminum film is added below circular patches array to form a meta-mirror.[30] The geometric parameters of p = 200 nm, t = 20 nm, d = 30 nm, and r = 45 nm are used throughout the following discussions. Owing to the complex evanescent coupling schematically illustrated in the bottom right panel, both the E_z component below the patches and the E_x component between two patches follow the catenary function. While E_z resembles the catenary fields plotted in Figure 1b, E_x is attributed to the evanescent coupling similar to that in Figure 1c.

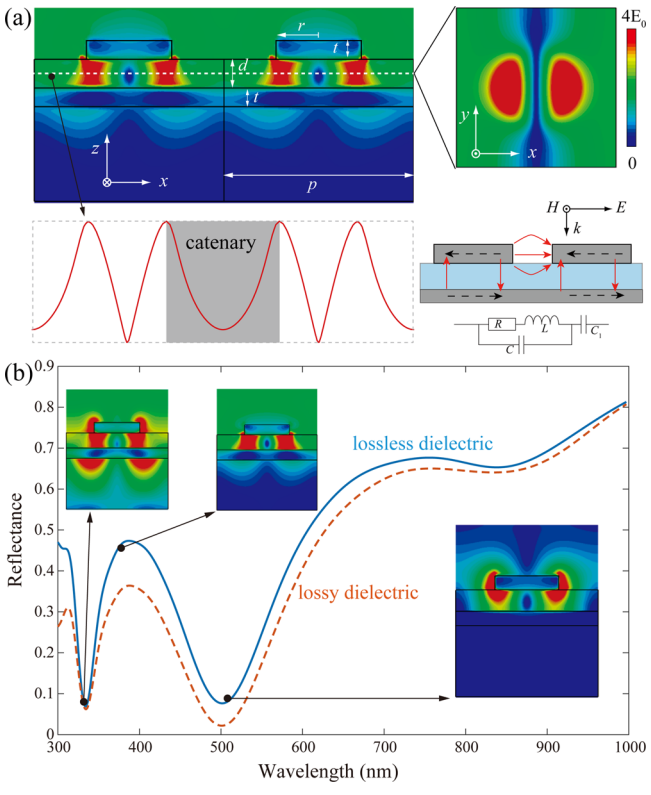

Figure 2. Averaged electric field distribution of double silts interference backed by a reflective metallic layer. Incident light is polarized along the x direction. (a) Fields in the xz- and xy-plane, as well as that indicated by the dashed line (λ = 375 nm). The bottom right panel shows the equivalent circuit model composed of parallel and serial circuits.[30] (b) Reflectance spectrum. The dashed curve corresponds to the case when a loss tangent of 0.05 is added into the dielectric. By comparing the two curves, it can be seen that the energy loss mainly occurs in the metallic parts. The inset shows the fields at corresponding wavelengths.

The interplay of vertical and horizontal catenary fields determines to some extent the optical properties (e.g., the reflection and absorption) of the metal−insulator−metal (MIM) structures.[30] Figure 2b illustrates that there are two reflection troughs locating at λ = 333 and 500 nm. By comparing the spectra of lossless and lossy dielectrics, it can be seen that the energy loss mainly comes from metal, accompanying with enhanced fields localized at the patches.[31] If we hope energy is not absorbed by the electrons in metal, the horizontal coupling between adjacent patches should be suppressed thus electric fields are confined in the dielectric layer, which is the case at the wavelength of 375 nm. One additional benefit of operating at 375 nm is the interference patterns may possess better uniformity along the z-direction and higher contrast in the x-direction, as shown in the inset of Figure 2b.

Applications. The catenary optical fields and EYI effect can be exploited for many important applications such as super-resolution lithography and spin-controlled photonics. First, since the MIM configuration is similar to the plasmonic cavity lens for nanolithography,[11,27] the intensity pattern can be directly recorded by the photoresist. In this case, the circular patches act as photomask while the dielectric acts as photoresist. Since the peak-to-peak distance between one pair of interference patterns is smaller than the diameter of the circular patch (90 nm in the simulations), the resolution of nanolithography is much smaller than the diffraction limit. Moreover, such structures can be easily fabricated using self-assembly of nanospheres.[32,33]

Figure 3 shows the intensity and phase distribution for a metallic patches array. Under CPL illumination at normal incidence, the E_z component forms ring patterns as a result of the symmetry of circular polarization. Note that the horizontal components E_x and E_y act as background for the ring-shaped patterns, which should be minimized by reducing the horizontal coupling between adjacent patches. The spiral phase shown in Figure 3c indicates there is a vertically polarized optical vortex induced by photonic spin−orbit interaction. However, different from the geometric phase resulting from polarization conversion from one circular state to its opposite one,[34] the phase shift should reduce by half:[35]

$$\Phi = \pm\varphi \tag{4}$$

where ± denotes left-handed circular polarization (LCP) and right-handed circular polarization (RCP) incidence, φ is the azimuthal angle. A simple explanation of the physical process is schematically illustrated in Figure 3d: if we consider CPL as a rotating linearly polarized wave, at each instantaneous time, the phase of E_z at the two sides of a patch would have a shift of π, which means that the absolute value of phase shift is coincident with the azimuthal angle.

The spin−orbit interaction at normal incidence has circularly symmetric intensity distribution. Under oblique

DOI: 10.1021/acsphotonics.8b00437
ACS Photonics 2018, 5, 3198−3204

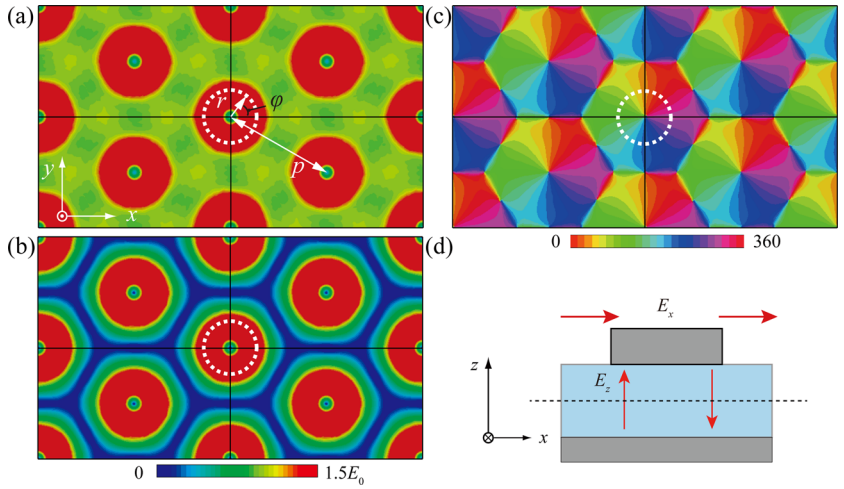

Figure 3. Fields distribution in the middle of the photoresist layer under CPL illumination. (a) Averaged amplitude for the electric fields. The dashed circle indicates the circular patch. (b, c) Averaged amplitude and phase for E_z. (d) Schematic of the spin−orbit interaction. Note that there is always a phase shift of π between E_z at the two sides of a given patch. The dashed line indicates the middle plane shown in (a)−(c).

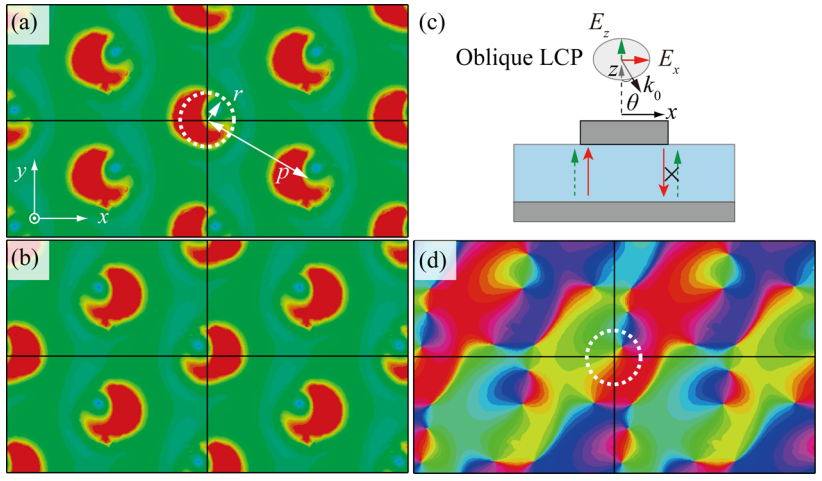

Figure 4. Fields distribution in the middle of photoresist layer under CPL illumination at an oblique incidence angle of θ. (a, b) Taiji fish-like averaged amplitudes for LCP and RCP illumination. (c) Schematic of the mechanism for spin Hall effect. The incident E_x component excites the antisymmetric E_z (solid red), while the incident E_z component excites the symmetric E_z (dashed green). (d) Phase distribution for E_z under LCP incidence.

incidence, however, asymmetric interference patterns could be realized. Figure 4 illustrates the fields distribution under LCP and RCP incidence at an angle of $\theta = 60°$ within the yz-plane. Obviously, the intensity distribution is dependent on the spin state, which could be regarded as one kind of optical spin Hall effect[36−38] or circular dichroism.[39,40] The dark center not only shifts along the y direction as a result of oblique incidence, but also has a horizontal spin-dependent shift owing to the spin−orbit interaction, which can be explained by considering the scattering process for two perpendicular components: As illustrated in Figure 4c, both the x and z components of the electric fields can excite the guiding modes in the photoresist layer, but with odd and even phase distribution, respectively. Taking LCP incidence as an example, the two components cancel each other at the right side and lead to a Taiji fish-like asymmetric intensity distribution shown in Figure 4a. For RCP incidence, the direction of the above process is flipped and a reversed intensity distribution is obtained in Figure 4b. To further investigate the spin−orbit interaction, the phase of E_z under LCP incidence is given in Figure 4d with an apparent offset of the phase center.

The polarization dependent interference in Figure 4b is similar to the spin-dependent guided modes excitation,[2,41,42] which redirects LCP and RCP light into opposite directions. However, unlike previous structures, the 2D slits proposed here ensure the generation of complex two-dimensional patterns, which have been demonstrated to be useful for polarizing optical applications.[43]

To further extend the concept of EYI, the interference of CPL is exploited to obtain more complex patterns. As shown in Figure 5a, the coherent addition of CPL would induce space-variant linear polarization, leading to inhomogeneously oriented anisotropic patterns in the photoresist layer. As a result, our proposed structures can convert polarization insensitive photoresist to be dependent on polarization, which is of particular importance in the recording of vectorial light fields. Strikingly, these anisotropic patterns can also generate geometric phase and redirect the incident CPL to one particular direction. Figure 5b,c illustrates the coherently

DOI: 10.1021/acsphotonics.8b00437
ACS Photonics 2018, 5, 3198−3204

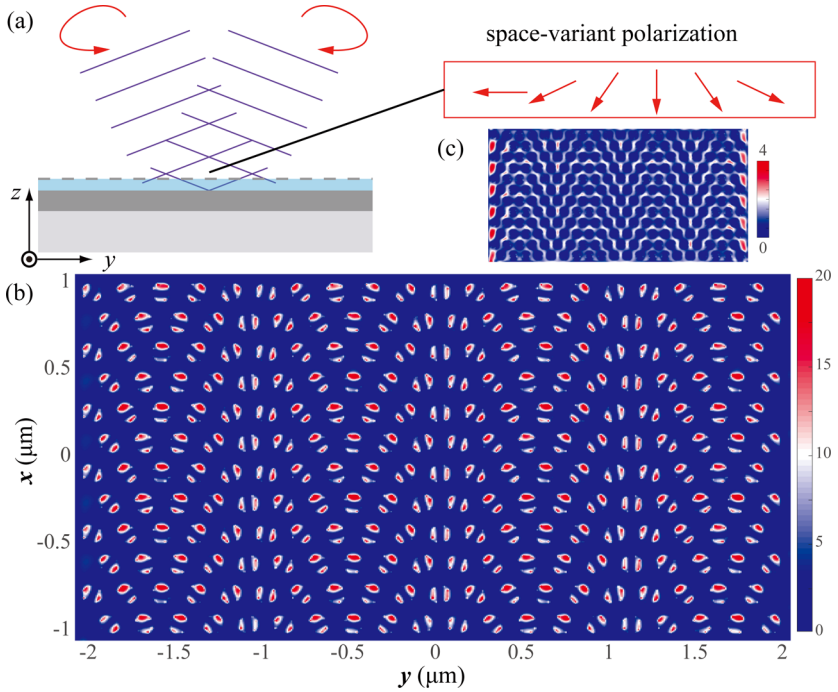

Figure 5. Interference of CPL in the photoresist. (a) Schematic of the interference configuration. The space-variant polarization is shown in the right panel. (b) Averaged intensity in the middle of the photoresist layer calculated by $(|E_x|^2 + |E_y|^2 + |E_z|^2)/2$. (c) Averaged horizontal intensity calculated by $(|E_x|^2 + |E_y|^2)/2$. Since the fields were calculated by adding two separate results obtained in CST MWS, the color map is shown in a way different from previous figures.

added fields illuminating at ±10° within the *yz* plane. Owing to the limited incidence angle, the asymmetric intensity distribution is not obvious, rendering a rotating dipole array with characteristic dimension smaller than 50 nm. Note that the horizontal electric fields shown in Figure 5c are negligible because the horizontal coupling is small.

CONCLUSIONS

In summary, we revisited the Young's double slits interference experiment with noble metals and photosensitive materials. Based on the analogy between mechanics and electromagnetics, we proposed the concept of catenary optical fields, which replace the normal sinusoidal functions as the solutions of Maxwell's equations. Following this concept, the competition between vertical and horizontal modes in modified double silts is analyzed and then utilized in plasmonic lithographic systems. By employing the photonic spin−orbit interaction, various functional structures including rings array, Taiji fish-like array, and space-variant rotating elements are formed. Through tuning the geometric shape of the top metallic patches as well as the phase profiles of the incident circular polarizations, more complex interference patterns may be realized for various functional devices.[44−47]

As a final remark, we stress that the catenary optical fields are a universal concept and have far-reaching applications in subwavelength coupled systems. While our discussion mainly concerns spin−orbit interaction and plasmonic nanolithography, the catenary optical fields also exist in other systems such as flat optical lenses, polarization converters, optical absorbers and even wireless power transfer devices.[8] We also noted that SPP is a manifestation of the spin−orbit momentum locking,[48] and the electric field lines in the uncoupled region (see inset of Figure 1a) follow the curves described by the "catenary of equal phase gradient".[34] Combining with the catenary subwavelength structures,[34,36,49] the catenary optics may deepen the understanding of subwavelength electromagnetics and find its application in much broader areas, including catenary antennas, catenary absorbers, and Engineering Optics 2.0.[8]

METHODS

Simulations. All calculations are performed with CST MWS. For transient solver, periodic (Figures 1 and 2), and open (Figure 5) boundary conditions are adopted for the unit cell and full model calculation. The minimal mesh is set to be $\lambda/100$ for Figures 1 and 2 and $\lambda/20$ for Figure 5. For frequency domain solver, Floquet port boundaries are adopted with a minimal mesh size of $\lambda/10$, which enables the calculation of periodic structures with CPL incidence (Figures 3 and 4).

AUTHOR INFORMATION

Corresponding Author

*E-mail: lxg@ioe.ac.cn.

ORCID

Xiangang Luo: 0000-0002-1401-1670

Notes

The authors declare no competing financial interest.

ACKNOWLEDGMENTS

This work was sponsored by the National Basic Research (973) Program of China under Grant No. 2013CBA01700 and the National Natural Science Foundation of China under Grant Nos. 61622508 and 61575201.

REFERENCES

(1) Crease, R. P. The Most Beautiful Experiment. *Phys. World* **2002**, *15*, 19.

DOI: 10.1021/acsphotonics.8b00437
ACS Photonics 2018, 5, 3198−3204

(2) Rodríguez-Fortuño, F. J.; Marino, G.; Ginzburg, P.; O'Connor, D.; Martínez, A.; Wurtz, G. A.; Zayats, A. V. Near-Field Interference for the Unidirectional Excitation of Electromagnetic Guided Modes. *Science* **2013**, *340*, 328−330.
(3) Zheludev, N. I. What Diffraction Limit? *Nat. Mater.* **2008**, *7*, 420−422.
(4) Pu, M.; Ma, X.; Li, X.; Guo, Y.; Luo, X. Merging Plasmonics and Metamaterials by Two-Dimensional Subwavelength Structures. *J. Mater. Chem. C* **2017**, *5*, 4361.
(5) Macleod, H. A. *Thin-Film Optical Filters*, 4th ed.; CRC Press: Boca Raton, FL, 2010.
(6) Boto, A. N.; Kok, P.; Abrams, D. S.; Braunstein, S. L.; Williams, C. P.; Dowling, J. P. Quantum Interferometric Optical Lithography: Exploiting Entanglement to Beat the Diffraction Limit. *Phys. Rev. Lett.* **2000**, *85*, 2733−2736.
(7) Boyd, R. W.; Dowling, J. P. Quantum Lithography: Status of the Field. *Quantum Inf. Process.* **2012**, *11*, 891−901.
(8) Luo, X. Subwavelength Optical Engineering with Metasurface Waves. *Adv. Opt. Mater.* **2018**, *6*, 1701201.
(9) Luo, X.; Ishihara, T. Surface Plasmon Resonant Interference Nanolithography Technique. *Appl. Phys. Lett.* **2004**, *84*, 4780−4782.
(10) Luo, X.; Ishihara, T. Subwavelength Photolithography Based on Surface-Plasmon Polariton Resonance. *Opt. Express* **2004**, *12*, 3055−3065.
(11) Gao, P.; Yao, N.; Wang, C.; Zhao, Z.; Luo, Y.; Wang, Y.; Gao, G.; Liu, K.; Zhao, C.; Luo, X. Enhancing Aspect Profile of Half-Pitch 32 nm and 22 nm Lithography with Plasmonic Cavity Lens. *Appl. Phys. Lett.* **2015**, *106*, 093110.
(12) Schouten, H. F.; Kuzmin, N.; Dubois, G.; Visser, T. D.; Gbur, G.; Alkemade, P. F. A.; Blok, H.; Hooft, G. W.; Lenstra, D.; Eliel, E. R. Plasmon-Assisted Two-Slit Transmission: Young's Experiment Revisited. *Phys. Rev. Lett.* **2005**, *94*, 053901.
(13) Shi, H.; Luo, X.; Du, C. Young's Interference of Double Metallic Nanoslit with Different Widths. *Opt. Express* **2007**, *15*, 11321−11327.
(14) Xu, T.; Wang, C.; Du, C.; Luo, X. Plasmonic Beam Deflector. *Opt. Express* **2008**, *16*, 4753−4759.
(15) Xu, T.; Zhao, Y.; Gan, D.; Wang, C.; Du, C.; Luo, X. Directional Excitation of Surface Plasmons with Subwavelength Slits. *Appl. Phys. Lett.* **2008**, *92*, 101501.
(16) Zia, R.; Brongersma, M. L. Surface Plasmon Polariton Analogue to Young's Double-Slit Experiment. *Nat. Nanotechnol.* **2007**, *2*, 426.
(17) Verslegers, L.; Catrysse, P. B.; Yu, Z.; Fan, S. Planar Metallic Nanoscale Slit Lenses for Angle Compensation. *Appl. Phys. Lett.* **2009**, *95*, 071112.
(18) Sun, J.; Wang, X.; Xu, T.; Kudyshev, Z. A.; Cartwright, A. N.; Litchinitser, N. M. Spinning Light on the Nanoscale. *Nano Lett.* **2014**, *14*, 2726−2729.
(19) Xu, T.; Du, C.; Wang, C.; Luo, X. Subwavelength Imaging by Metallic Slab Lens with Nanoslits. *Appl. Phys. Lett.* **2007**, *91*, 201501.
(20) Lee, B.; Kim, S.; Kim, H.; Lim, Y. The Use of Plasmonics in Light Beaming and Focusing. *Prog. Quantum Electron.* **2010**, *34*, 47−87.
(21) Li, Y.; Liu, F.; Xiao, L.; Cui, K.; Feng, X.; Zhang, W.; Huang, Y. Two-Surface-Plasmon-Polariton-Absorption Based Nanolithography. *Appl. Phys. Lett.* **2013**, *102*, 063113.
(22) Liu, H.; Luo, Y.; Kong, W.; Liu, K.; Du, W.; Zhao, C.; Gao, P.; Zhao, Z.; Wang, C.; Pu, M.; et al. Large Area Deep Subwavelength Interference Lithography with a 35 nm Half-Period Based on Bulk Plasmon Polaritons. *Opt. Mater. Express* **2018**, *8*, 199−209.
(23) Marcuse, D. *Light Transmission Optics*, 2nd ed.; Van Nostrand Reinhold Company: New York, 1982.
(24) Joannopoulos, J. D.; Johnson, S. G.; Winn, J. N.; Meade, R. D. *Photonic Crystals: Molding the Flow of Light*, 2nd ed.; Princeton University Press: Princeton and Oxford, 2008.
(25) Pendry, J. B.; Martin-Moreno, L.; Garcia-Vidal, F. J. Mimicking Surface Plasmons with Structured Surfaces. *Science* **2004**, *305*, 847−848.
(26) Luo, X. Principles of Electromagnetic Waves in Metasurfaces. *Sci. China: Phys., Mech. Astron.* **2015**, *58*, 594201.
(27) Luo, X. Plasmonic Metalens for Nanofabrication. *Natl. Sci. Rev.* **2018**, *5*, 137−138.
(28) Liu, L.; Gao, P.; Liu, K.; Kong, W.; Zhao, Z.; Pu, M.; Wang, C.; Luo, X. Nanofocusing of Circularly Polarized Bessel-type Plasmon Polaritons with Hyperbolic Metamaterials. *Mater. Horiz.* **2017**, *4*, 290−296.
(29) Pu, M.; Chen, P.; Wang, Y.; Zhao, Z.; Huang, C.; Wang, C.; Ma, X.; Luo, X. Anisotropic Meta-Mirror for Achromatic Electromagnetic Polarization Manipulation. *Appl. Phys. Lett.* **2013**, *102*, 131906.
(30) Pu, M.; Hu, C.; Wang, M.; Huang, C.; Zhao, Z.; Wang, C.; Feng, Q.; Luo, X. Design Principles for Infrared Wide-Angle Perfect Absorber Based on Plasmonic Structure. *Opt. Express* **2011**, *19*, 17413−17420.
(31) Feng, Q.; Pu, M.; Hu, C.; Luo, X. Engineering the Dispersion of Metamaterial Surface for Broadband Infrared Absorption. *Opt. Lett.* **2012**, *37*, 2133−2135.
(32) Liu, H.; Zhao, X.; Yang, Y.; Li, Q.; Lv, J. Fabrication of Infrared Left-Handed Metamaterials via Double Template-Assisted Electrochemical Deposition. *Adv. Mater.* **2008**, *20*, 2050−2054.
(33) Kim, E. S.; Kim, Y. M.; Choi, K. C. Surface Plasmon-Assisted Nano-Lithography with a Perfect Contact Aluminum Mask of a Hexagonal Dot Array. *Plasmonics* **2016**, *11*, 1337−1342.
(34) Pu, M.; Li, X.; Ma, X.; Wang, Y.; Zhao, Z.; Wang, C.; Hu, C.; Gao, P.; Huang, C.; Ren, H.; et al. Catenary Optics for Achromatic Generation of Perfect Optical Angular Momentum. *Sci. Adv.* **2015**, *1*, e1500396.
(35) Guo, Y.; Pu, M.; Zhao, Z.; Wang, Y.; Jin, J.; Gao, P.; Li, X.; Ma, X.; Luo, X. Merging Geometric Phase and Plasmon Retardation Phase in Continuously Shaped Metasurfaces for Arbitrary Orbital Angular Momentum Generation. *ACS Photonics* **2016**, *3*, 2022−2029.
(36) Luo, X.; Pu, M.; Li, X.; Ma, X. Broadband Spin Hall Effect of Light in Single Nanoapertures. *Light: Sci. Appl.* **2017**, *6*, e16276.
(37) Zhou, J.; Qian, H.; Hu, G.; Luo, H.; Wen, S.; Liu, Z. Broadband Photonic Spin Hall Meta-Lens. *ACS Nano* **2018**, *12*, 82−88.
(38) Zhang, F.; Pu, M.; Li, X.; Gao, P.; Ma, X.; Luo, J.; Yu, H.; Luo, X. All-Dielectric Metasurfaces for Simultaneous Giant Circular Asymmetric Transmission and Wavefront Shaping Based on Asymmetric Photonic Spin−Orbit Interactions. *Adv. Funct. Mater.* **2017**, *27*, 1704295.
(39) Ma, X.; Huang, C.; Pu, M.; Hu, C.; Feng, Q.; Luo, X. Multi-Band Circular Polarizer Using Planar Spiral Metamaterial Structure. *Opt. Express* **2012**, *20*, 16050−16058.
(40) Liu, Y.; Guo, Q.; Liu, H.; Liu, C.; Song, K.; Yang, B.; Hou, Q.; Zhao, X.; Zhang, S.; Navarro-Cía, M. Circular-Polarization-Selective Transmission Induced by Spin-Orbit Coupling in a Helical Tape Waveguide. *Phys. Rev. Appl.* **2018**, *9*, 054033.
(41) Lin, J.; Mueller, J. P. B.; Wang, Q.; Yuan, G.; Antoniou, N.; Yuan, X.-C.; Capasso, F. Polarization-Controlled Tunable Directional Coupling of Surface Plasmon Polaritons. *Science* **2013**, *340*, 331−334.
(42) Rodríguez-Fortuño, F. J.; Barber-Sanz, I.; Puerto, D.; Griol, A.; Martínez, A. Resolving Light Handedness with an On-Chip Silicon Microdisk. *ACS Photonics* **2014**, *1*, 762−767.
(43) Cui, Y.; Kang, L.; Lan, S.; Rodrigues, S.; Cai, W. Giant Chiral Optical Response from a Twisted-Arc Metamaterial. *Nano Lett.* **2014**, *14*, 1021−1025.
(44) Qin, F.; Ding, L.; Zhang, L.; Monticone, F.; Chum, C. C.; Deng, J.; Mei, S.; Li, Y.; Teng, J.; Hong, M.; et al. Hybrid Bilayer Plasmonic Metasurface Efficiently Manipulates Visible Light. *Sci. Adv.* **2016**, *2*, e1501168.
(45) Li, X.; Chen, L.; Li, Y.; Zhang, X.; Pu, M.; Zhao, Z.; Ma, X.; Wang, Y.; Hong, M.; Luo, X. Multicolor 3D Meta-Holography by Broadband Plasmonic Modulation. *Sci. Adv.* **2016**, *2*, e1601102.
(46) Liu, Y.; Liu, C.; Song, K.; Li, M.; Zhao, X. A Broadband High-Transmission Gradient Phase Discontinuity Metasurface. *J. Phys. D: Appl. Phys.* **2018**, *51*, 095103.

DOI: 10.1021/acsphotonics.8b00437
ACS Photonics 2018, 5, 3198−3204

(47) Pu, M.; Li, X.; Guo, Y.; Ma, X.; Luo, X. Nanoapertures with Ordered Rotations: Symmetry Transformation and Wide-Angle Flat Lensing. *Opt. Express* **2017**, *25*, 31471−31477.
(48) Bliokh, K. Y.; Smirnova, D.; Nori, F. Quantum Spin Hall Effect of Light. *Science* **2015**, *348*, 1448−1451.
(49) Li, X.; Pu, M.; Zhao, Z.; Ma, X.; Jin, J.; Wang, Y.; Gao, P.; Luo, X. Catenary Nanostructures as Highly Efficient and Compact Bessel Beam Generators. *Sci. Rep.* **2016**, *6*, 20524.

DOI: 10.1021/acsphotonics.8b00437
ACS Photonics 2018, 5, 3198−3204